Giri, Ashutosh; Niemelä, Janne Petteri; Tynell, Tommi; Gaskins, John T.; Donovan, Brian F.; Karppinen, Maarit; Hopkins, Patrick E.

Heat-transport mechanisms in molecular building blocks of inorganic/organic hybrid superlattices

Published in:
Physical Review B

DOI:
10.1103/PhysRevB.93.115310

Published: 16/03/2016

Document Version
Publisher's PDF, also known as Version of record

Heat-transport mechanisms in molecular building blocks of inorganic/organic hybrid superlattices

Ashutosh Giri,[1] Janne-Petteri Niemelä,[2] Tommi Tynell,[2] John T. Gaskins,[1] Brian F. Donovan,[1] Maarit Karppinen,[2] and Patrick E. Hopkins[1,*]

[1]*Department of Mechanical and Aerospace Engineering, University of Virginia, Charlottesville, Virginia 22904, USA*

[2]*Department of Chemistry, Aalto University, FI-00076 Aalto, Finland*

(Received 30 September 2015; revised manuscript received 19 February 2016; published 16 March 2016)

Nanomaterial interfaces and concomitant thermal resistances are generally considered as atomic-scale planes that scatter the fundamental energy carriers. Given that the nanoscale structural and chemical properties of solid interfaces can strongly influence this thermal boundary conductance, the ballistic and diffusive nature of phonon transport along with the corresponding phonon wavelengths can affect how energy is scattered and transmitted across an interfacial region between two materials. In hybrid composites composed of atomic layer building blocks of inorganic and organic constituents, the varying interaction between the phononic spectrum in the inorganic crystals and vibronic modes in the molecular films can provide a new avenue to manipulate the energy exchange between the fundamental vibrational energy carriers across interfaces. Here, we systematically study the heat transfer mechanisms in hybrid superlattices of atomic- and molecular-layer-grown zinc oxide and hydroquinone with varying thicknesses of the inorganic and organic layers in the superlattices. We demonstrate ballistic energy transfer of phonons in the zinc oxide that is limited by scattering at the zinc oxide/hydroquinone interface for superlattices with a single monolayer of hydroquinone separating the thicker inorganic layers. The concomitant thermal boundary conductance across the zinc oxide interfacial region approaches the maximal thermal boundary conductance of a zinc oxide phonon flux, indicative of the contribution of long wavelength vibrations across the aromatic molecular monolayers in transmitting energy across the interface. This transmission of energy across the molecular interface decreases considerably as the thickness of the organic layers are increased.

DOI: 10.1103/PhysRevB.93.115310

I. INTRODUCTION

The introduction of material interfaces in solid nanocomposites has provided the opportunity for user-defined thermal transport in nanosystems through manipulation of the fundamental carriers of heat. The inclusion of these interfaces gives rise to both phonon-boundary scattering, effectively reducing the thermal conductivity of the solid due to classical size effects [1] and/or partial transmission of thermal energy across the interface driving the thermal boundary conductance [2,3]. To atomistically manipulate the phonon thermal conductivity of a nanosystem with a high density of material interfaces, an understanding of the interplay and relationship of phonon-boundary scattering and thermal boundary conductance across the interfaces must be understood [4]. Given that the structural and chemical properties of solid interfaces can strongly influence the thermal boundary conductance [5], the ballistic or diffusive nature of phonon transport along with the corresponding phonon wavelengths [6] can affect how energy is scattered and/or transmitted across an interfacial region between two materials. This ballistic to diffusive crossover of phonon transport and energy transmission across an atomically thin interface is poorly understood.

The consideration of these ballistic and diffusive interfacial phonon energy transport processes has major implications for the development of novel nanomaterials for applications such as thermoelectric energy conversion [7–9], where careful placement of interfaces has proven to be useful in efficiently lowering the phononic conductivity while still maintaining electronic conductivity. As an example of a novel class of nanocomposites of recent interest, hybrid organic/inorganic nanomaterials grown by a combined alternation of atomic layer deposition (ALD) and molecular layer deposition (MLD) have exhibited enhanced electrical, optical, magnetic, and mechanical functionalities compared to conventional organic or inorganic materials [10–13]. For example, using this ALD/MLD technique, inorganic/organic superlattices (SLs) have shown promise as potential thermoelectric materials [14,15]. However, paramount in advancing ALD/MLD hybrid structures for use in thermoelectric, or other applications, is an understanding of the phonon transport and scattering processes in these materials; referring to ALD/MLD SLs, this requires understanding phonon scattering at the ALD/MLD boundary, and its correlation with phonon transmission and resulting boundary conductance across the molecular interface. There have been limited previous works focusing on measurements of thermal conductivity of ALD/MLD grown materials [14,16–18]. Given the high density of molecular interfaces in these composite systems, advances in the thermophysics of these materials rely on understanding the thermal conductance across the molecular interfaces.

Given the recent interest in thermal transport in organic-based nanocomposites [19–23] and heat transport across molecular interfaces [24–30], systematically studying the thermal conductivity of a series of ALD/MLD-grown hybrid SLs also provides an ideal platform to advance our understanding of phonon scattering at, and heat transfer across, thin molecular interfaces. These high-quality hybrid nanosystems also provide ideal materials to understand the heat transfer mechanisms in organic/inorganic SLs, and the interplay between phonon-boundary scattering and thermal boundary conductance across interfaces of identical materials separated by a well-defined molecular layer.

*phopkins@virginia.edu

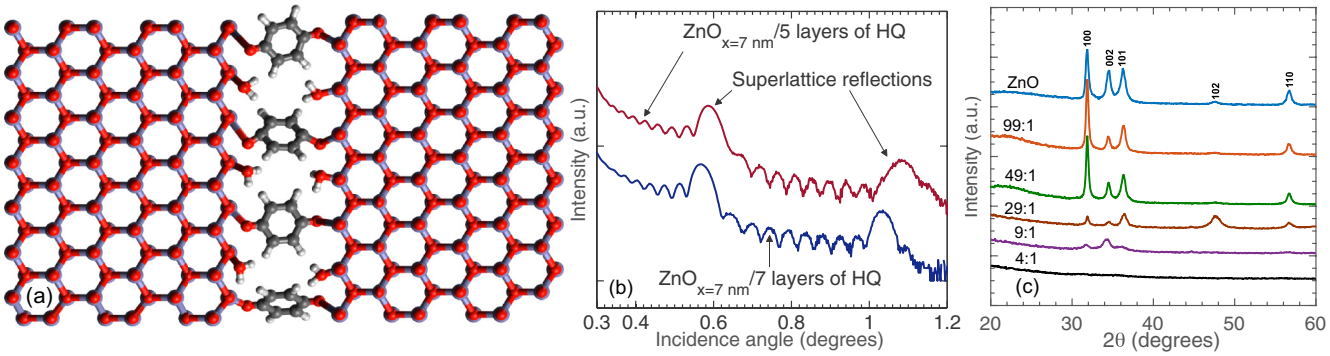

FIG. 1. (a) 2D Schematic representation of the ZnO_x/HQ SL. (b) Characteristic XRR patterns showing SL reflections for ZnO_x/HQ with $x = 7.0$ nm with 5 and 7 layers of HQ separating the 7-nm-thick inorganic constituents. (c) Characteristic grazing incidence x-ray diffraction (GIXRD) patterns for the control sample and hybrid SLs with varying x. The peaks in the XRD patterns for the hybrid SLs fit to the typical hexagonal wurtzite structure of ZnO (indexed accordingly). There are no shifts in the position of the peaks for the hybrid SLs with ALD:MLD cycle ratios of 99:1, 49:1, 29:1, and 9:1, suggesting that the introduction of the organic monolayers do not affect the crystallinity of the ZnO phase.

In this manuscript, we study the phonon transport mechanisms in a series of ALD/MLD grown SL thin films composed of multiple layers of zinc oxide/hyroquinone. The series of SLs include period thicknesses varying from 0.7 to 13.1 nm with monolayers of hydroquinone (HQ) interspersed in between the thicker inorganic layers of ZnO. We also study the effect of the organic layer thickness on the thermal transport across these SLs by investigating a set of samples fabricated by varying the MLD cycles while keeping the thickness of the inorganic layers constant. Additionally, we compare our results of the ZnO-based SLs to that of titanium dioxide (TiO_2)-based SLs (Refs. [17] and [18]), to scope the generality of our results.

We measure the thermal conductivity, κ, of the SLs providing a platform to study the role of organic interface density on phonon scattering at the inorganic/organic interface and thermal boundary conductance across the inorganic/organic/inorganic interface. We show that thermal transport in ZnO-based hybrid SLs with monolayers of HQ at an interface can be described as a boundary-scattering-dominated process that is limited by the period length, thereby reducing the thermal conductance of the crystalline inorganic layer. Our model suggests that nearly the entire spectrum of phonons in the inorganic layer is limited by scattering at the inorganic/organic interface. As an alternative analysis, we determine a mean thermal boundary conductance across the inorganic/organic/inorganic interfaces. The reduction in the transmission of phonons across the ZnO/HQ/ZnO interface leads to an overall reduction in the thermal conductivity of the SLs compared to the thermal conductivity of a homogeneous ZnO thin film. Furthermore, as we increase the thickness of the organic layers in the SLs, we observe a reduction in the phonon transmission across the inorganic/organic/inorganic interfaces in the hybrid SLs, which results in a reduction in the overall thermal conductivity of the composite.

II. EXPERIMENTAL DETAILS

$(ZnO)_x$/HQ (where x is the period thickness of the SL) thin films of five different periodicities were grown via ALD/MLD on single-crystal MgO substrates, an illustration of the structure is shown in Fig. 1(a). An additional set of samples were fabricated with three different numbers of HQ layers (i.e., 3, 5, and 7 layers) in between the ZnO layers with $x = 7.0$ nm. Diethyl zinc and water were used as precursors for the ZnO layers, while hydroquinone was used for the MLD layers. The depositions were performed at 220°C and consisted of 605 ALD/MLD cycles with an ALD:MLD cycle ratio of 99:1, 49:1, 29:1, 9:1, and 4:1. Control sample of ZnO thin film with similar thickness as the hybrid SL samples were also fabricated via ALD. X-ray reflectivity (XRR) measurements with a PANalytical X'Pert Pro X-ray diffractometer were used to determine the thickness of the films (∼100 nm) and the SL periods, x. The measured thicknesses are tabulated in Table S1 of the Supplemental Material [31]. A more detailed description of the film fabrication and characterization can be found in Ref. [32].

Characteristic XRR patterns for $ZnO_{x=7.0\,nm}/5$ and 7 layers of HQ are shown in Fig. 1(b). The film thickness dictates the small fringes corresponding to the interference minima and maxima of the reflected beam film-air and film-substrate interfaces, respectively [33]. The XRR also includes interference maxima with higher intensities that represent constructive interference from the periodic introduction of the organic layers. Figure 1(c) shows the characteristic grazing incidence x-ray diffraction (GIXRD) patterns for the SLs. Typically, the peaks in the XRD patterns were found to fit the typical ZnO hexagonal wurzite structure. As is clear from Fig. 1(c), there is almost no change in the position of the peaks for the SLs, suggesting that the crystallinity of the ZnO phase is preserved with the inclusion of the HQ layers. However, the intensity of the peaks for the SLs with higher number of organic monolayers (and ALD:MLD cycle ratios of 29:1, 9:1, and 4:1) are reduced compared to the purely ALD grown ZnO film, implying that the crystallinity is hindered to some extent for the inorganic constituents due to the organic monolayers. For the SL with the thinnest inorganic constituent, the XRD pattern suggests that the inorganic constituents are amorphous.

We use the time domain thermoreflectance technique (TDTR) to measure the thermal properties of the samples. The appropriate analysis procedure for these TDTR measurements has been previously discussed in detail by several groups

[34–36]. Prior to TDTR measurements, we metalize the samples with a thin Al layer deposited via electron beam evaporation at 6×10^{-6} Torr. In our TDTR experimental setup, laser pulses emanate from a Ti:Sapphire oscillator with an 80 MHz repetition rate and are energetically split into pump and probe paths. The train of ultrashort pump pulses thermally stimulate the Al metal transducer and time-delayed probe pulses measure the change in the thermoreflectance of the sample due to the decay of the deposited thermal energy. We modulate the pump path at 8.8 MHz and monitor the ratio of the in-phase to out-of-phase signal of the probe beam from a lock-in amplifier ($-V_{in}/V_{out}$) for up to 5 ns after the initial heating event. To ensure negligible sensitivity to in-plane transport, our pump and probe spot sizes were focused to $1/e^2$ radii values of 30 and 9 μm, respectively. We measure the thermoreflectance response of each sample in a liquid nitrogen cooled cryostat from 78 to 300 K. We perform several TDTR scans at different locations to ensure repeatability in our measurements. We determine the thermal conductivities and thermal boundary conductances in our samples by fitting our TDTR data to the thermal model that accounts for pulse accumulation from the Ti:Sapphire oscillator [34–36]. The thickness of the Al transducer layer is measured via picosecond acoustics [37].

Initially, we fit the time domain thermoreflectance (TDTR) data for our ALD grown control sample with a model that accounts for thermal diffusion in a three-layer system by fitting for thermal boundary conductances across the Al/ZnO and ZnO/Al_2O_3 interfaces. All other parameters in our thermal model such as the thermal conductivities and heat capacities of the constituent layers are taken from literature [38–41]; note, due to small thermal resistance of pure ZnO, we are negligibly sensitive to the thermal conductivity of the ZnO thin film and our TDTR data on these control samples are dominated by the thermal boundary conductances (h_K) at the Al/ZnO and ZnO/Al_2O_3 interfaces, as shown in Fig. 2(a) and discussed in detail below.

To evaluate the thermophysical properties of interest in our control samples, namely the thermal boundary conductances across the Al/ZnO and ZnO/Al_2O_3 interfaces, we must determine the appropriate range of pump-probe delay times to fit the thermal model to the experimental data, in which the thermal model is extremely sensitive to changes in h_K [36,42]. To determine these interface resistances, we use a combination of the in-phase response and the ratio of the in-phase to out-of-phase responses over various pump-probe time delays, due to relative sensitivities to the thermophysical properties of interest in this system. The sensitivity of the in-phase signal to various thermal properties is defined by

$$S_a = \frac{\partial \ln(-V_{in})}{\partial \ln(a)}, \quad (1)$$

where a is the thermophysical parameter of interest and V_{in} is directly proportional to the response of the thermoreflectance signal recorded by the lock-in amplifier. Figure 2(a) shows the sensitivites of V_{in} to the thermophysical properties of interest in our ZnO control sample at 300 K. The sensitivity to h_K for the Al/ZnO interface is relatively large and very dynamic for the first nanosecond time delay at both 78 and 300 K. In this time frame, the sensitivities of the other parameters are

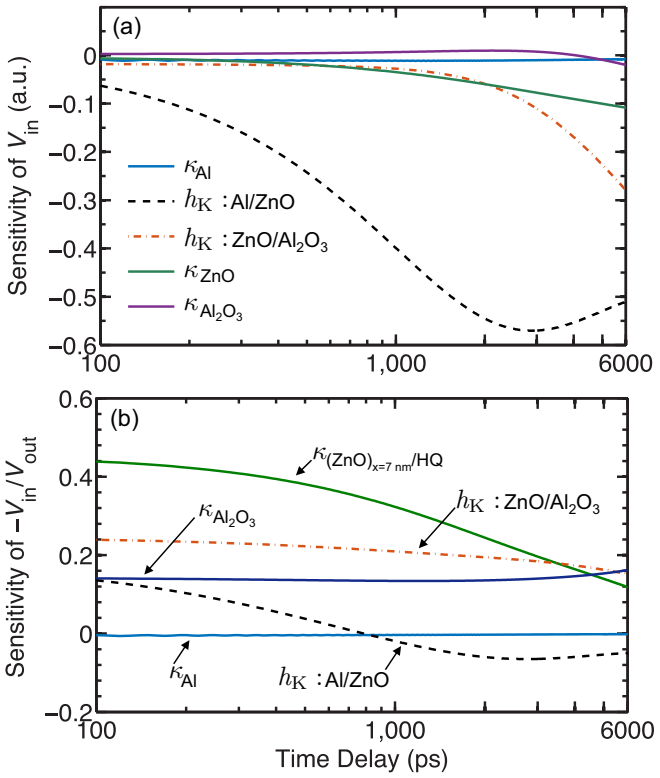

FIG. 2. (a) Sensitivities of the (a) in-phase signal (for a purely ALD grown ZnO thin film) and (b) ratio of the in-phase and out-of-phase signals (for the $(ZnO)_{x=7\,nm}/HQ$ film) to the thermal boundary conductances at Al/ZnO and ZnO/Al_2O_3 interfaces and thermal conductivities of Al, ZnO, and Al_2O_3.

minimal and therefore will not affect the thermal response of the control sample. Therefore, we fit the in-phase signal with the thermal model by iterating the h_K for the Al/ZnO interface and all the other parameters are held constant for 1-ns time delay. We note that since fitting the in-phase response of the TDTR signal requires scaling our model to the data at a fixed delay time (which we choose as 100 ps), we become completely insensitive to thermophysical properties that have flat sensitivities in the time domain, further enhancing our accuracy in determining h_K over our specified time delay. Similarly, we determine the h_K for the ZnO/Al_2O_3 interface by fitting the in-phase signal in the range of 2–5 ns while using the h_K for the Al/ZnO interface determined from the first 1-ns time delay fit. We discuss this fitting approach in more detail in the Supplemental Material.

The measured thermal boundary conductances from the control sample are used as input parameters for thermal conductivity analyses of the superlattice samples $[(ZnO)_x/HQ]$. We fit the ratio of the in-phase and out-of-phase signals ($-V_{in}/V_{out}$) to the three-layer thermal model to determine the thermal conductivity of the superlattice films. For these fits, we use the thermal boundary conductances determined from our in-phase analyses, leaving the only unknown parameter in these measurements as the thermal conductivity of the $(ZnO)_x/HQ$ films. Figure 2(b) shows the sensitivity of the ratio to the various parameters in our three-layer model for the $(ZnO)_{x=7\,nm}/HQ$ film. An error of 15% in h_K

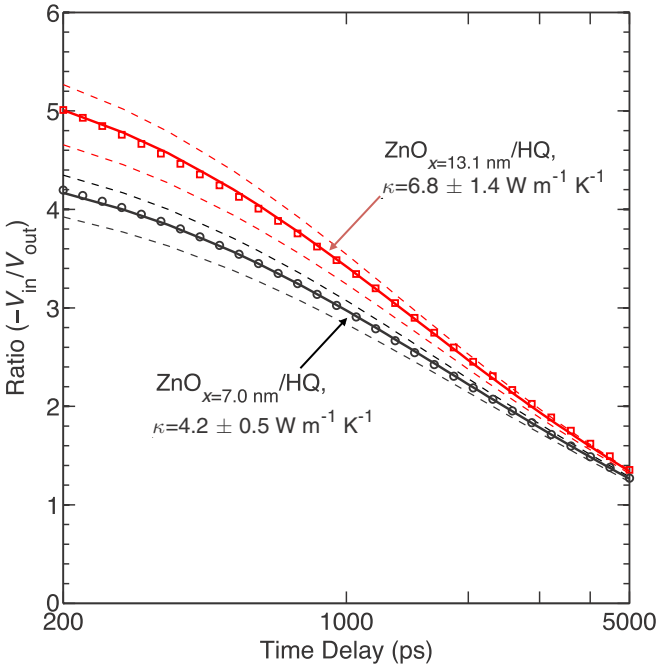

FIG. 3. Sample data and best-fit curves for the $(ZnO)_{x=13.1\,nm}/HQ$ (red squares) and $(ZnO)_{x=7.0\,nm}/HQ$ (black circles) along with uncertainties (dotted lines) at room temperature.

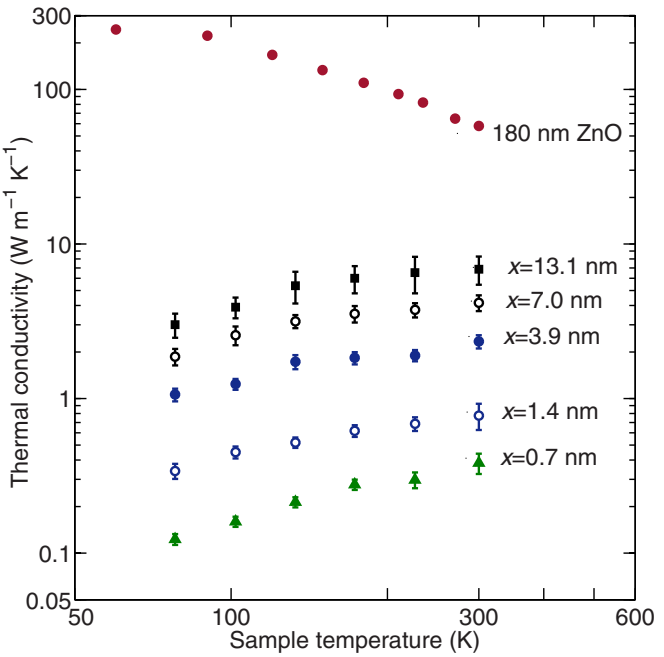

FIG. 4. Measured thermal conductivities as a function of temperature for $(ZnO)_x/HQ$ SLs with varying x. The error bars include uncertainties due to repeatability, Al thickness measurement, and uncertainties in the parameters used in the thermal model. Also plotted are the thermal conductivities for a 180-nm ALD-grown homogenous ZnO film taken from Ref. [39].

for the Al/ZnO interface propagates to an error of ∼1.5% and ∼0.8% on the measured thermal conductivities of the $(ZnO)_{x=13.1\,nm}/HQ$ and $(ZnO)_{x=7.0\,nm}/HQ$ samples at room temperature, respectively. However, an error of 15% in h_K for the ZnO/Al_2O_3 interface causes an error of ∼13% and ∼7% in the measured conductivities for $(ZnO)_{x=13.1\,nm}/HQ$ and $(ZnO)_{x=7.0\,nm}/HQ$ samples at room temperature, respectively. This is a major source of uncertainty reported for our measurements. The fits to the TDTR data along with the uncertainties (dashed lines) for the samples $(ZnO)_{x=7.0\,nm}/HQ$ and $(ZnO)_{x=13.1\,nm}/HQ$ at 300 K are shown in Fig. 3.

III. RESULTS AND DISCUSSIONS

Figure 4 shows the measured thermal conductivities for the $(ZnO)_x/HQ$ SLs with varying x at different sample temperatures. The thermal conductivities of these SLs demonstrate more than a tenfold decrease compared to the results for an ALD-grown homogeneous ZnO thin film [39], as shown in Fig. 4. The inclusion of higher interface densities and the reduction in the inorganic layer thickness results in the reduction of the thermal conductivities of these hybrid SLs.

To describe the results in Fig. 4, we consider the thermal transport in these hybrid samples being described by a phonon flux in the inorganic material that is limited only by phonon/boundary scattering at the inorganic/organic interface. In other words, we assume that the overall thermal conductivities of the SL films are minimally affected by scattering mechanisms in the bulk of the inorganic constituent (such as phonon-defect or phonon-phonon scattering in the individual layers). Therefore, the thermal transport is limited by the combination of the phonon flux, q, in the inorganic layers and the thickness, x, of the layers (i.e., x = period thickness of the SLs). The phonon flux in the inorganic layer can be approximated by [43]

$$q = \frac{1}{8\pi^2}\sum_j \int_{k_1} \hbar\omega k^2 v_j f\, dk, \tag{2}$$

where j is the polarization, ω is the phonon frequency, $\hbar$ is Planck's constant, f is the Bose-Einstein distribution, and v is the group velocity. Equation (1) assumes an isotropic, spherical Brillouin zone to predict the heat flux in the inorganic ZnO layers. We note that this assumption correctly predicts the volumetric heat capacity of ZnO (further details of the assumptions and our calculations are provided in the Supplemental Material). With the flux, q, determined from the phonon dispersion, the effective thermal conductivity of the SLs, which is dictated by the period thickness x, is given by

$$\kappa_{\text{effective}} = \frac{1}{3}\int C_k v_k dk x = \frac{\partial q}{\partial T}x, \tag{3}$$

where T is temperature and C_k is the spectral phonon heat capacity. Equation (3) assumes that phonon transport in the inorganic layer is ballistic and that the phonons scatter only at boundaries that restore local thermodynamic equilibrium. As such, our discussion and analyses assume that the interfacial organic boundaries are considered to be reflectionless and black, and the phonon flux is assumed to thermalize at these boundaries. Calculations of Eq. (3) for ZnO at two temperatures as a function of x are shown in Fig. 5. For these calculations, we use all 12 branches of the bulk phonon dispersion relation for ZnO in the $\Gamma \rightarrow M$ direction, as calculated in Ref. [44] via *ab initio* methods. The measured

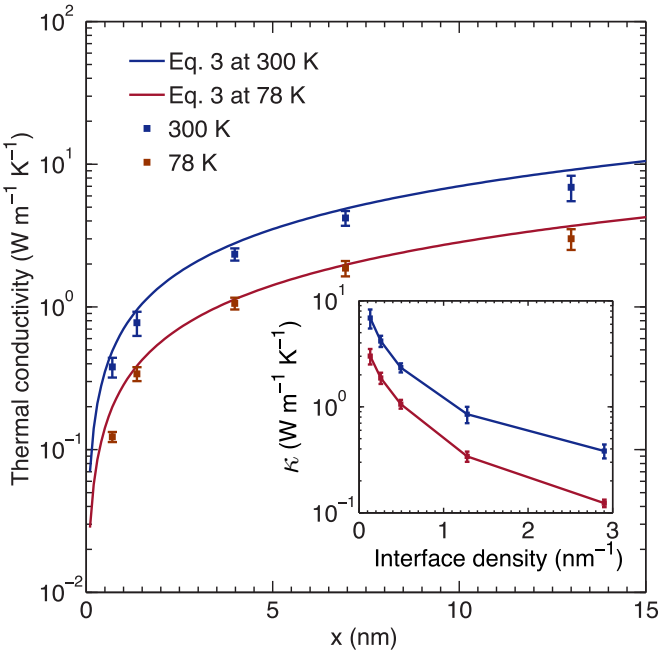

FIG. 5. Thermal conductivity as a function of the inorganic layer thickness for SLs with single HQ layers at 78 and 300 K. Along with that, the predicted thermal conductivities as a function of SL period thickness calculated from Eq. (2) at 78 and 300 K are also shown. The effective thermal conductivity model assuming only phonon-boundary scattering at the HQ-layer interface described in Eq. (3) provides reasonable agreement with the measured thermal conductivities for these SLs. (Inset) The thermal conductivity for these hybrid SLs is inversely proportional to the ZnO/HQ/ZnO interface density.

thermal conductivities at 78 and 300 K for the SLs show good agreement with our calculations of Eq. (3), supporting our assertion that size effects in the inorganic layers of the hybrid SLs limit thermal transport. This analysis assumes that the entire spectrum of phonon mean free paths in the ZnO layer is limited by scattering at the inorganic/organic/inorganic interface.

The drastic reduction in the thermal conductivity values decreasing period in the SLs is clearly seen by the inverse relationship of κ with ZnO/HQ/ZnO interface density as shown in the inset of Fig. 5. To scope the generality of these results to hybrid SLs, we compare the measured thermal conductivity of 3.1 ± 0.2 W m^{-1} K^{-1} for a $(TiO_2)_x$/HQ SL with $x = 15.5$ nm at room temperature to the thermal conductivity measurement for a homogeneous TiO_2 thin film (5.2 ± 0.3 W m^{-1} K^{-1}) [17,18]. The reduction in thermal conductivity for the TiO_2-based SL is in line with the results reported for the $(ZnO)_x$/HQ SLs. This reduction in the thermal conductivity due to the periodic monolayers is consistent with the decrease in thermal conductivity with increased interface density in inorganic SLs [45,46].

As pointed out in purely inorganic SLs, the monotonic decrease in thermal conductivity due to increased interface density (and linearly increasing thermal resistance with increasing interface density) is due to incoherent scattering, where the phonons behave as particles and lose their phase information by scattering at the internal boundaries [45,46]. Ravichandran *et al.* [45] have shown that by increasing the interface density (decreasing period thicknesses) beyond the incoherent regime, the phonon dispersion in inorganic SLs can be altered by mini-band formation, which effectively preserves the coherent nature of phonon transport in these SLs. An alternative wave nature of phonon transport in inorganic SLs has also been demonstrated by Luckyanova *et al.* [47], where they varied the total thickness of the inorganic SL films while keeping the SL period thicknesses constant and showed an increase in the thermal conductivity. Our results for the hybrid SLs are consistent with the particle nature of phonon transport (or the incoherent scattering regime) as demonstrated by the monotonically decreasing thermal conductivity with increasing interface densities (see inset of Fig. 5).

The appreciable agreement between our measured values for a wide range of inorganic layer thicknesses and that predicted by the model in Eq. (3) (as shown in Fig. 5) suggests that the phonon flux in the inorganic layer is mostly ballistic and the phonon mean free path is limited by the ZnO layer thicknesses. However, for thicker inorganic layers, where phonon-phonon scattering in the bulk of the inorganic layer creates a temperature gradient along the layer, the validity of Eq. (3) in describing thermal transport in these SLs is questionable. In fact, this is exemplified by the disagreement between the prediction of Eq. (3) for $x = 13.1$ nm and the experimentally measured κ for $(ZnO)_{x=13.1\,nm}$/HQ. Therefore, by describing the thermal transport by Eq. (3), we have considered the thermal conductivities of these hybrid SLs to be driven by a ballistic phonon flux limited by scattering at the inorganic/organic interface, which clearly breaks down as the ZnO thickness increases. Therefore, to study the validity and range of applicability of this hypothesis, we consider an alternative analysis of our results in Figs. 4 and 5 by considering the reduction in thermal conductivity to be driven by a thermal boundary conductance across the inorganic/organic/inorganic interface. This approach will give quantitative insight into the role of phonon transmission across the inorganic/organic/inorganic interface on our measured thermal conductivities. Note, as we are not able to separate the individual resistances due to scattering at the ZnO/HQ boundaries and the internal scattering in the HQ layer, we couple these scattering mechanisms into a lumped resistance in our discussions and analysis presented below.

In the typical semiclassical picture of thermal boundary conductance across solid interfaces (i.e., the acoustic or diffuse mismatch models [2,48,49]), a mismatch in acoustic properties or vibrational density of states limits the interfacial phonon transmission and therefore restricts the phonon flux that transmits across the organic-based interfaces. The acoustic mismatch model (AMM) considers phonons as plane waves and the lattice as a continuum solid and assumes specular reflection and transmission of phonon energy at the interface, whereas the diffuse mismatch model (DMM) disregards this complete specularity at the interface. These models could potentially offer complementary, yet alternative insight into the mechanisms driving the large reduction in the measured thermal conductivity of these hybrid SLs, and elucidate the role of the organic monolayers and their intrinsic vibrational properties on phonon transport. We model the thermal boundary conductance (h_K) through the organic interface, which is

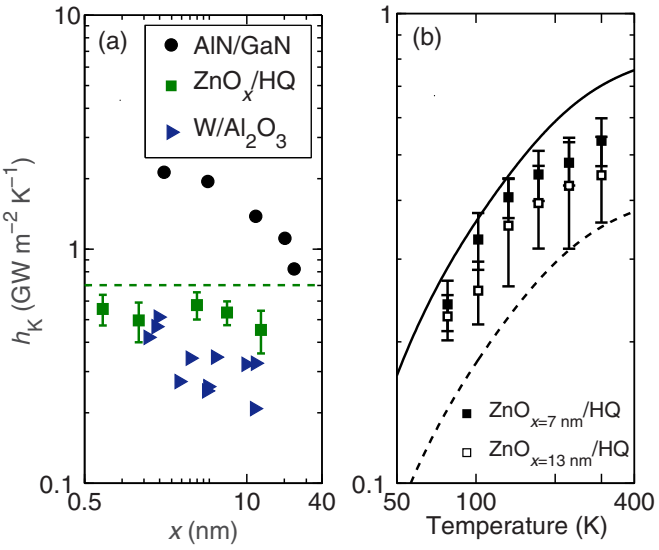

FIG. 6. (a) The mean thermal boundary conductances of interfaces in ZnO_x/HQ SLs derived from thermal conductivity measurements shown in Fig. 4. Also plotted are the mean conductances of interfaces in W/Al_2O_3 SLs [51] and AlN/GaN SLs [52] for comparison. (b) The mean thermal boundary conductances derived for $x = 7.0$ and 13.1 nm as a function of temperature for the ZnO-based SLs. The calculations of maximum conductance in ZnO with phonon transmission coefficient equal to unity are also shown. Also included for comparison is the calculation of the DMM for a ZnO/ZnO interface (i.e., 50% transmission of the ZnO phonon flux).

described by the temperature derivative of the phonon flux [as described in Eq. (2)] with the inclusion of a transmission coefficient ($\zeta_{1\to2}$) from side 1 to 2 (from inorganic, through the organic monolayer, and emitted into the next inorganic layer). The thermal boundary conductance is defined based on the temperature of the incident and emitted phonons, and therefore it predicts a finite interfacial conductance (as opposed to an infinite conductance or zero thermal boundary resistance) for an imaginary interface composed of the same material [50]. This conductance occurs when $\zeta_{1\to2} = 1$ and all available phonon modes are transmitted from side 1 to 2 of the imaginary interface in the crystal. We note that by this definition, the maximum possible thermal boundary conductance for an imaginary interface is solely limited by the phonon flux that impinges upon the interface. Alternatively, assuming an interface between two materials that causes diffusive scattering, this maximum limit is described by a transmission of $\zeta = 0.5$.

To consider the possibility of the thermal boundary conductance across the inorganic/organic/inorganic interface-limiting the thermal transport across the SLs, we model h_K across the ZnO/HQ/ZnO interface assuming maximal phonon transmission. This assumption implies that the phonon transmission from the ZnO across the HQ is unimpeded by any properties of the HQ; that is, we assume $\zeta_{1\to2} = 1$. For these calculations, we make the same assumptions for ZnO density of states and phonon velocities as in Eq. (2). Calculation of this maximal conductance at room temperature for a ZnO phonon flux is shown in Fig. 6(a) (dashed line). In most real nanosystems, due to both a mismatch of vibrational density of states and imperfections around the interfacial regions, the transmission coefficient is not unity (for a review of thermal boundary conductance dictated by various interfacial conditions, readers are referred to Ref. [5]). For this reason, the measured values of h_K in the literature have never exceeded this maximum thermal boundary conductance for any interface.

From the measured thermal conductivities in our hybrid SLs, we derive the mean thermal boundary conductance across the individual ZnO/HQ/ZnO interfaces with a series resistor model, which assumes that phonons can only scatter at the ZnO/HQ/ZnO interfaces (consistent with our previous analysis where we assume that the phonon flux is only scattered at the ZnO/HQ boundaries). We calculate the mean conductance across the HQ layers as $h_K = 1/R_K = (\kappa_{ZnO_x/HQ} n)/d$, where n is the number of inorganic/organic/inorganic interfaces and d is the total thickness of the hybrid films. To reiterate, this formulation of $1/R_K$ implies that the resistance due to the individual ZnO/HQ interfaces and the intrinsic resistance of the organic molecules comprising the interface are lumped as a single resistor.

Figure 6(a) shows the mean thermal conductance for ZnO/HQ/ZnO interfaces as a function of the inorganic layer thickness (hollow squares). Two aspects of the results for the conductance calculations shown in Fig. 6(a) are worth noting. First, the values of the mean conductances for these SLs among the various samples are agreeable within the uncertainties, regardless of the ZnO/HQ/ZnO interface density. This suggests that the series resistor model used to derive these conductances is applicable for our hybrid SLs with single HQ layers, and our previous assumption and discussion regarding fully thermalizing (i.e., black) inorganic/organic boundaries is supported. Along with the results for the hybrid SLs, we also plot the mean conductances derived from thermal conductivity measurements for W/Al_2O_3 [51] and AlN/GaN[52] SLs. Contrary to our hybrid SLs, the mean conductances in these inorganic based SLs increase with decreasing period thicknesses. In Ref. [52], this increase in h_K for the AlN/GaN SLs was attributed to phonons with long wavelengths carrying the majority of heat.

The second aspect worth noting is that the mean conductances derived are close to the maximum conductance with $\zeta = 1$. We demonstrate this consistency over a wide range of temperatures, shown in Fig. 6(b), which plots h_K calculated for ZnO/HQ/ZnO interface as a function of temperature for the two SLs with $x = 13.1$ and 7.0 nm. The appreciable agreement between these values and the conductance in ZnO is consistent with the analysis in Fig. 5 (treating all phonon mean free paths being limited by scattering at the ZnO/HQ/ZnO interface), as mentioned above. This agreement also suggests that a large portion of the phonon modes in the ZnO transmits ballistically across the ZnO/HQ/ZnO interface, implying relatively minor intrinsic thermal resistance in the molecular layer. While the relatively minor disagreement between the maximal conductance [Fig. 6(b), solid line] and the data could imply some level of phonon-vibron interactions in the HQ layer, more rigorous computational models are necessary to draw quantitative conclusions regarding these diffusive scattering processes in the molecule.

In order to quantify the contribution of the vibrational properties of the organic layer on phonon transmission across the ZnO/HQ/ZnO interfacial region, we calculate the average phonon transmissions from the results in Fig. 6(b) (comparing the maximal conductance model to the data) and find interfacial transmissions of ∼76% for the $(ZnO)_{7.0\,nm}$/HQ sample and ∼65% for the $(ZnO)_{13.1\,nm}$/HQ sample at room temperature. This deviation from "perfect" transmission of phonons could be due to the fact that heat flux carried by phonons with wavelengths longer than the organic molecular chain lengths are unaffected by the organic layer, whereas phonons with wavelengths on the order of and smaller than the molecular lengths are scattered due to the vibrational properties of the molecules (as discussed in more detail in the Supplemental Material). We note that 75–91% of the phonon flux in ZnO is carried by phonons with wavelengths longer than the average thickness of the HQ layer (Supplemental Material), supporting this hypothesis. We note that this hypothesis is consistent with previous works suggesting that at interfaces, the transmission of phonon wavelengths greater than the characteristic length scales of nanoscale structures and asperities at solid interfaces are not affected by these nonidealities [5,6,52–55]. More rigorous computational simulations are necessary to study this hypothesis in more detail, which includes a greater understanding of diffusive vibrational scattering in single-molecule thick films as previously mentioned.

One of the factors driving the high phonon transmission values across ZnO/HQ/ZnO interfaces could be due to the high-quality interfaces within the SLs and the precise control over the thicknesses of the inorganic layers achieved via the layer-by-layer deposition of the ALD/MLD technique [17,56]. At the inorganic/organic interfaces, it has been shown through first principles study that the HQ molecules are most probably attached to every other surface Zn site (50% surface coverage) [57]. This implies that we cannot rule out the possibility of ZnO growth at the lateral interstitial positions, which could affect the phonon energy transmission across these inorganic/organic/inorganic interfaces; in principle, this could happen if the physical size of the HQ would prevent itsÕ reaction with all the Diethyl zinc terminated surface sites. However, the systematically lower densities (predicted from XRR measurements and reported in the Supplemental Materials), with increasing number of MLD cycles, suggest that the presence of interstitial ZnO within the organic layers is unlikely.

The implication of large thermal transmission across the single HQ layer assumes that there is no mismatch of acoustic impedance or vibrational spectra encountered by the impinging ZnO flux on the HQ monolayer. Although this would be true for a pure ZnO/ZnO interface in which phonons are specularly scattered, this clearly would not be the case if considering phonon thermal conductance limited by transmission across the ZnO/HQ/ZnO interface due to properties of the HQ. To exemplify this more quantitatively, we performed molecular dynamics simulations on a plane of HQ molecules to obtain the power spectral density. The power spectral density is compared to the $D(\omega)$ spectrum for bulk ZnO calculated from the phonon dispersion [44], and as expected, the relatively discrete modes in the phonon frequencies calculated for the HQ layer do not completely overlap the $D(\omega)$ for ZnO (Fig. S6 in Supplemental Material). Note, we do not attempt to separate the scattering at the ZnO/HQ boundary from the internal scattering within the organic monolayers from our MD simulations, which is beyond the scope of this study. However, from our predicted phonon density of states for a confined HQ layer mimicking a 50% surface coverage, we can infer that under the typical DMM picture of phonon transmission from the ZnO across the HQ and into the next ZnO layer, a HQ-limited transmission seems implausible.

To scope the generality of the discussions presented above, we derive the conductance across the TiO_2/HQ/TiO_2 from the thermal conductivity measurement for the TiO_2-based SL at room temperature [17] and compare the value to the result for a control sample without the HQ layers (Al/TiO_2/MgO). We determine $h_K = 430 \pm 78$ MW m^{-2} K^{-1} for TiO_2/HQ/TiO_2 interface, lower than that of the ZnO-based SLs at room temperature. From this, we determine the phonon transmission across the TiO_2/HQ/TiO_2 interface to be ∼41%. Further calculations of the spectral heat flux as a function of the wave-vector for TiO_2 (Supplemental Material) demonstrates that the percent heat flux carried by phonons with wavelengths shorter than ∼6–7 Å in TiO_2 is ∼53–62%, in reasonable agreement with the ∼41% transmission determined for the TiO_2-based sample.

In order to investigate the role of molecular vibrations on the phonon-scattering mechanisms, we measured the thermal conductivities of SLs with 3, 5, and 7 layers of HQ molecules interspersed between $x = 7.0$-nm-thick ZnO layers at room temperature (see top panel of Fig. 7 for depictions of unit cells [57]). As shown in Fig. 7(a), increasing the number of MLD cycles for the SLs decreases the thermal conductivity monotonically. Note, the prediction of Eq. (3) for $x = 7$ nm does not agree with the measurements for thicker HQ layers, which we ascribe to ZnO phonons scattering in the organic layers due to the vibrational properties of the thicker HQ layers. To further quantify the role of the vibrational resistance on these composite structures, we plot the mean thermal boundary resistance across the ZnO/HQ/ZnO interface as a function of number of molecular layers in Fig. 7(b) as calculated from the series resistor model. The linear trend in resistance as the HQ layer is increased from 3 to 7 layers suggests that the internal diffusive scattering in the organic layer plays a significant role in impeding thermal transport for SLs with greater than or equal to 3 layers of HQ in between the inorganic layers. We note that from GIXRD measurements, we do not observe a significant reduction in the crystallinity of the inorganic constituents due to inclusion of the thicker HQ layers, implying that the reduction in thermal conductivities of these structures with 3 to 7 HQ layers is mainly due to scattering at the thicker HQ layers.

We gain quantitative support for this result by calculating the average phonon transmission from the ZnO across the HQ layer using the approach discussed previously [transmissions shown in Fig. 7(b)]. Increasing the MLD cycles from a monolayer to 3 HQ layers drastically reduces the transmission from 76% to 53%. Upon further increase in the number of HQ layers to 5 and 7, the transmissions reduce to 28% and 23%, respectively. Previous studies on the length-dependent vibrational transport in molecular chains have mostly focused

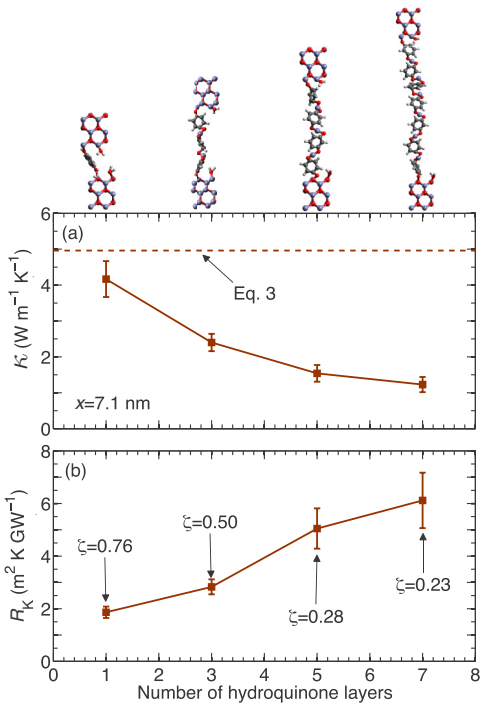

FIG. 7. Top panel depicts unit cells with increasing number of hydroquinone molecules. (a) Thermal conductivity measurements at room temperature as a function of the number of MLD cycles performed. Calculation of Eq. (2) for the inorganic layer thickness is also shown for comparison. The measured thermal conductivity for the SLs deviate from the prediction of Eq. (3) as the HQ layer thicknesses increase. (b) Effective resistances of inorganic/organic/inorganic interfaces with varying number of hydroquinone layers derived from the thermal conductivities shown in (a).

on self-assembled monolayers of aliphatic alkane chains [27,58–60]. Most of these studies have concluded that the conductance across molecular chains is insensitive to the length of the hydrocarbon chains, particularly in Ref. [60], it is shown that the conductance is constant for chain lengths >20 carbon atoms. However, for shorter chain lengths, theoretical calculations by Segal *et al.* [60] and experimental data by Meier *et al.* [59] suggest that conductance is maximum for a chain length of up to 4 carbon atoms and decreases with increasing number of carbon atoms thereafter to a certain chain length. From our results, the drastic reduction in phonon transmission coefficients with thicker HQ layers compared to that of the SLs with a monolayer of HQ molecule could be due to the diffusive nature of vibrational transport in the longer chain molecules. However, as pointed out previously, we cannot comprehensively separate the resistances due to inorganic/organic interface scattering and the internal scattering in the molecular layers. Therefore, we do not attempt to separate the intrinsic thermal conductivity of the individual organic layers from the overall thermal conductivity of the hybrid films.

IV. CONCLUSIONS

We conclude that the heat transfer mechanisms in hybrid SLs with single molecular layers are strongly influenced by phonon-boundary scattering, where nearly the entire spectrum of phonon mean free paths in the inorganic layer is limited by scattering at the inorganic/organic interface. The resulting thermal conductivities of these hybrid nanostructures are mainly limited by the ZnO phonon flux and period spacing of the inorganic layers. Our analysis suggests that the phonon flux in the inorganic layer, which scatters at the inorganic/organic interface, limits the thermal conductivity of these nanostructures. The mean conductances derived from the thermal conductivity measurements also suggest that scattering at the molecular layer interfaces accounts for the majority of the reduction in the thermal conductivity of hybrid SLs with single organic layers. By considering this as a thermal boundary conductance limited processes, we hypothesize that phonons with wavelengths greater than the organic layer thickness are transmitted across the organic layers after scattering at the inorganic/organic interface; these phonon wavelengths make up >75% of the phonon flux in the ZnO, which offers a concomitant picture of the heat transfer processes in inorganic/organic hybrid composites. By increasing the thickness of the MLD-grown layer, we observe a significant reduction in the phonon transmission across the thicker molecular layers as compared to the thermal conductance across the single organic layers. The linear trend in thermal resistance with number of molecular layers suggests a diffusive scattering process in the MLD-grown organic layer, which offers a robust opportunity for more focused theoretical or computational studies to pinpoint the size effects in vibronic scattering in aromatic molecules.

ACKNOWLEDGMENTS

P.E.H. appreciates support from the United States Army Research Office (Grant No. W911NF-13-1-0378). M.K. appreciates support from the Aalto Energy Efficiency Research Programme and the European Research Council under the European Union's Seventh Framework Programme (Grant No. FP/2007-2013)/ERC Advanced Grant Agreement (No. 339478).

[1] G. Chen, *Nanoscale Energy Transport and Conversion: A Parallel Treatment of Electrons, Molecules, Phonons, and Photons (MIT-Pappalardo Series in Mechanical Engineering)* (Oxford University Press, USA, 2005).

[2] E. T. Swartz and R. O. Pohl, Rev. Mod. Phys. **61**, 605 (1989).

[3] P. L. Kapitza, Zh. Eksp. Teor. Fiz. **11**, 1 (1941).

[4] It is important to note that the reduction in the thermal conductivity of a material due to phonon boundary scattering may not be entirely correlated to the intrinsic thermal boundary conductance between two solids and is influenced by ballistic transport and phonon mean free paths incident upon the interface, as has been shown both computationally [61] and experimentally [52] .

[5] P. E. Hopkins, ISRN Mech. Eng. **2013**, 682586 (2013).

[6] R. Cheaito, J. T. Gaskins, M. E. Caplan, B. F. Donovan, B. M. Foley, A. Giri, J. C. Duda, C. J. Szwejkowski, C. Constantin, H. J. Brown-Shaklee, J. F. Ihlefeld, and P. E. Hopkins, Phys. Rev. B **91**, 035432 (2015).

[7] N. Mingo, D. Hauser, N. P. Kobayashi, M. Plissonnier, and A. Shakouri, Nano Lett. **9**, 711 (2009).

[8] S. J. Poon and K. Limtragool, J. Appl. Phys. **110**, 114306 (2011).

[9] J. Tang, H.-T. Wang, D. H. Lee, M. Fardy, Z. Huo, T. P. Russell, and P. Yang, Nano Lett. **10**, 4279 (2010).

[10] Y. Chujo, Curr. Opin. Solid State Mater. Sci. **1**, 806 (1996).

[11] P. Judeinstein and C. Sanchez, J. Mater. Chem. **6**, 511 (1996).

[12] B. Yoon, B. H. Lee, and S. M. George, J. Phys. Chem. C **116**, 24784 (2012).

[13] K.-H. Yoon, K.-S. Han, and M.-M. Sung, Nanoscale Res. Lett. **7**, 71 (2012).

[14] T. Tynell, A. Giri, J. Gaskins, P. E. Hopkins, P. Mele, K. Miyazaki, and M. Karppinen, J. Mater. Chem. A **2**, 12150 (2014).

[15] T. Tynell, I. Terasaki, H. Yamauchi, and M. Karppinen, J. Mater. Chem. A **1**, 13619 (2013).

[16] J. Liu, B. Yoon, E. Kuhlmann, M. Tian, J. Zhu, S. M. George, Y.-C. Lee, and R. Yang, Nano Lett. **13**, 5594 (2013).

[17] J.-P. Niemelä, A. Giri, P. E. Hopkins, and M. Karppinen, J. Mater. Chem. A **3**, 11527 (2015).

[18] A. Giri, J.-P. Niemelä, C. J. Szwejkowski, M. Karppinen, and P. E. Hopkins, Phys. Rev. B **93**, 024201 (2016).

[19] W.-L. Ong, S. Majumdar, J. A. Malen, and A. J. H. McGaughey, J. Phys. Chem. C **118**, 7288 (2014).

[20] W.-L. Ong, S. M. Rupich, D. V. Talapin, A. J. H. McGaughey, and J. A. Malen, Nat. Mater. **12**, 410 (2013).

[21] M. D. Losego, I. P. Blitz, R. A. Vaia, D. G. Cahill, and P. V. Braun, Nano Lett. **13**, 2215 (2013).

[22] J. P. Feser, E. M. Chan, A. Majumdar, R. A. Segalman, and J. J. Urban, Nano Lett. **13**, 2122 (2013).

[23] J. C. Duda, P. E. Hopkins, Y. Shen, and M. C. Gupta, Phys. Rev. Lett. **110**, 015902 (2013).

[24] M. D. Losego, M. E. Grady, N. R. Sottos, D. G. Cahill, and P. V. Braun, Nat. Mater. **11**, 502 (2012).

[25] P. E. Hopkins, M. Baraket, E. V. Barnat, T. E. Beechem, S. P. Kearney, J. C. Duda, J. T. Robinson, and S. G. Walton, Nano Lett. **12**, 590 (2012).

[26] R. Y. Wang, R. A. Segalman, and A. Majumdar, Appl. Phys. Lett. **89**, 173113 (2006).

[27] Z. Wang, J. A. Carter, A. Lagutchev, Y. K. Koh, N.-H. Seong, D. G. Cahill, and D. D. Dlott, Science **317**, 787 (2007).

[28] Z. Wang, D. G. Cahill, J. A. Carter, Y. K. Koh, A. Lagutchev, N.-H. Seong, and D. D. Dlott, Chem. Phys. **350**, 31 (2008).

[29] P. J. O'Brien, S. Shenogin, J. Liu, P. K. Chow, D. Laurencin, P. H. Mutin, M. Yamaguchi, P. Keblinski, and G. Ramanath, Nat. Mater. **12**, 118 (2013).

[30] Y. Jin, C. Shao, J. Kieffer, K. P. Pipe, and M. Shtein, J. Appl. Phys. **112**, 093503 (2012).

[31] See Supplemental Material at http://link.aps.org/supplemental/10.1103/PhysRevB.93.115310 for information on experimental and analytical details.

[32] T. Tynell and M. Karppinen, Thin Solid Films **551**, 23 (2014).

[33] J.-P. Niemelä and M. Karppinen, Dalton Trans. **44**, 591 (2015).

[34] D. G. Cahill, Rev. Sci. Instrum. **75**, 5119 (2004).

[35] A. J. Schmidt, X. Chen, and G. Chen, Rev. Sci. Instrum. **79**, 114902 (2008).

[36] P. E. Hopkins, J. R. Serrano, L. M. Phinney, S. P. Kearney, T. W. Grasser, and C. T. Harris, J. Heat Transfer **132**, 081302 (2010).

[37] G. Tas and H. J. Maris, Phys. Rev. B **49**, 15046 (1994).

[38] V. P. Elena, R. Dobrovinskaya Leonid, and A. Lytvynov, *Sapphire: Material, Manufacturing, Applications*, 1st ed. (Springer, Berlin, 2009).

[39] J. Alvarez-Quintana, E. Martínez, E. Pérez-Tijerina, S. A. Pérez-García, and J. Rodríguez-Viejo, J. Appl. Phys. **107**, 063713 (2010).

[40] C. Ho, *Thermal Conductivity of the Elements: A Comprehensive Review* (American Chemical Society and the American Institute of Physics for the National Bureau of Standards, New York, 1975).

[41] C. Klingshirn, A. Waag, A. Hoffmann, and J. Geurts, *Zinc Oxide: From Fundamental Properties Towards Novel Applications*, Vol. 120 (Springer, Berlin, 2010).

[42] R. M. Costescu, M. A. Wall, and D. G. Cahill, Phys. Rev. B **67**, 054302 (2003).

[43] J. C. Duda, P. M. Norris, and P. E. Hopkins, J. Heat Transfer **133**, 074501 (2011).

[44] J. Serrano, F. J. Manjón, A. H. Romero, A. Ivanov, M. Cardona, R. Lauck, A. Bosak, and M. Krisch, Phys. Rev. B **81**, 174304 (2010).

[45] J. Ravichandran, A. K. Yadav, R. Cheaito, P. B. Rossen, A. Soukiassian, S. J. Suresha, J. C. Duda, B. M. Foley, C.-H. Lee, Y. Zhu, A. W. Lichtenberger, J. E. Moore, D. A. Muller, D. G. Schlom, P. E. Hopkins, A. Majumdar, R. Ramesh, and M. A. Zurbuchen, Nat. Mater. **13**, 168 (2014).

[46] P. M. Norris, N. Q. Le, and C. H. Baker, J. Heat Transfer **135**, 061604 (2013).

[47] M. N. Luckyanova, J. Garg, K. Esfarjani, A. Jandl, M. T. Bulsara, A. J. Schmidt, A. J. Minnich, S. Chen, M. S. Dresselhaus, Z. Ren, E. A. Fitzgerald, and G. Chen, Science **338**, 936 (2012).

[48] W. A. Little, Can. J. Phys. **37**, 334 (1959).

[49] I. M. Khalatnikov, J. Exp. Theor. Phys. (Z. Eksp. Teor. Fiz.) **22**, 687 (1952).

[50] G. Chen and T. Zeng, Microscale Thermophys. Eng. **5**, 71 (2001).

[51] R. M. Costescu, D. G. Cahill, F. H. Fabreguette, Z. A. Sechrist, and S. M. George, Science **303**, 989 (2004).

[52] Y. K. Koh, Y. Cao, D. G. Cahill, and D. Jena, Adv. Funct. Mater. **19**, 610 (2009).

[53] P. E. Hopkins, J. C. Duda, C. W. Petz, and J. A. Floro, Phys. Rev. B **84**, 035438 (2011).

[54] J. C. Duda and P. E. Hopkins, Appl. Phys. Lett. **100**, 111602 (2012).

[55] P. E. Hopkins, L. M. Phinney, J. R. Serrano, and T. E. Beechem, Phys. Rev. B **82**, 085307 (2010).

[56] P. Sundberg and M. Karppinen, Beilstein J. Nanotechnol. **5**, 1104 (2014).

[57] A. J. Karttunen, T. Tynell, and M. Karppinen, J. Phys. Chem. C **119**, 13105 (2015).

[58] J. C. Duda, C. B. Saltonstall, P. M. Norris, and P. E. Hopkins, J. Chem. Phys. **134**, 094704 (2011).

[59] T. Meier, F. Menges, P. Nirmalraj, H. Hölscher, H. Riel, and B. Gotsmann, Phys. Rev. Lett. **113**, 060801 (2014).

[60] D. Segal, A. Nitzan, and P. Hänggi, J. Chem. Phys. **119**, 6840 (2003).

[61] R. E. Jones, J. C. Duda, X. W. Zhou, C. J. Kimmer, and P. E. Hopkins, Appl. Phys. Lett. **102**, 183119 (2013).